

This is the **accepted version** of the article:

Muñoz Enano, Jonathan; Vélez Rasero, Paris; Gil Barba, Marta; [et al.].
«Differential-mode to common-mode conversion detector based on rat-race hybrid couplers : analysis and application to differential sensors and comparators». IEEE Transactions on Microwave Theory and Techniques, Vol. 68, issue 4 (April 2020), p. 1312-1325. DOI 10.1109/TMTT.2019.2955676

This version is available at <https://ddd.uab.cat/record/221398>

under the terms of the  **CC BY** license

Differential-Mode to Common-Mode Conversion Detector Based on Rat-Race Hybrid Couplers: Analysis and Application to Differential Sensors and Comparators

Jonathan Muñoz-Enano, *Student Member IEEE*, Paris Vélez, *Member IEEE*, Marta Gil, Javier Mata-Contreras, and Ferran Martín, *Fellow IEEE*

Abstract—A microwave device able to detect differential-mode to common-mode conversion (or vice versa) in a four-port balanced circuits is proposed. For mode conversion detection, the balanced circuit should be fed by a differential-mode signal, generated by means of a rat-race balun from a single-ended signal. By connecting the pair of output ports of the balanced circuit under test to one of the two pairs of isolated ports of a second rat-race coupler, conversion to the common-mode (if it exists) can be detected, and recorded in the Σ -port. Since the signal level at the output (single-ended) port depends on mode conversion efficiency, the complete two-port structure, including the pair of rat-race couplers plus the balanced circuit in between, can be used as a comparator or differential microwave sensor based on mode conversion. In such sensor, the working principle is symmetry disruption (caused, e.g., by an asymmetric dielectric load), and the output variable is the transmission coefficient, related to the level of asymmetry. A detailed analysis, considering an arbitrary unbalanced four-port test structure (to account for symmetry disruption), is carried out. Then, such analysis is particularized to the case of a pair of unbalanced and uncoupled matched lines, and the conditions for sensitivity optimization are obtained. Finally, a differential sensor and comparator based on a pair of balanced (and meandered) matched lines, designed according to the guidelines for sensitivity optimization, is fabricated and validated.

Index Terms—Common-mode, differential-mode, differential sensor, microstrip, microwave sensor, rat-race coupler.

I. INTRODUCTION

THE INTEREST for differential-mode (or balanced) microwave circuits has increased in recent years due to their high immunity to electromagnetic interference (EMI), noise and crosstalk (at least as compared to single-ended circuits) [1],[2]. A critical aspect in balanced circuits is mode conversion, typically caused by an imperfect balance and responsible for the generation of (undesired) common

mode noise, which in turn may affect device performance. For that reason, many efforts have been dedicated to the design of common-mode filters [2],[3]-[22], as well as to the design of balanced circuits with inherent common-mode rejection [23]-[57]. Nevertheless, mode conversion in balanced circuits should be avoided, or minimized as much as possible, by ensuring accurate fabrication processes that prevent from symmetry disruption (imbalances).

Balanced structures have been also applied to the design of differential sensors [58]-[62]. Such sensors offer a high level of robustness against cross sensitivities related to environmental conditions (e.g., temperature, moisture, etc.), as far as ambient factors are seen as common-mode stimulus. Typically, these sensors consist of a pair of mirror structures (independent sensors), sensitive to the variable to be sensed (measurand). Sensing principle is symmetry truncation caused by a difference in the measurand in both sensing parts, one for the reference (REF) measurand (well known), and the other one for the measurand under test (MUT). The output variable is usually inferred from the difference between a certain magnitude (sensitive to the measurand) recorded in the REF and MUT sensing parts. It should be mentioned that other similar sensors which are also based on symmetry disruption but cannot be considered true differential sensors, have been recently reported [63]-[77].

A useful parameter to detect symmetry imbalances caused by differences between the REF and MUT measurand in differential sensors is the cross-mode transmission coefficient. This parameter, sensitive to mode conversion, has been used as output variable in differential sensors based on pairs of balanced transmission lines loaded with resonant elements (the sensing element) [78]-[80]. In [79],[80], such sensors were applied to the determination of solute concentration in very diluted solutions, by adding fluidic channels on top of the resonant elements. Very competitive resolution and sensitivity, as compared to the reported literature to date [81]-[85], was achieved. However, in the sensors reported in [79],[80], four-port devices, the output variable (cross-mode transmission coefficient) was obtained from the measurement of the mixed-mode S-parameters [1],[2],[86],[87], which involves either a four-port vector network analyzer, or multiple two-port measurements of single-ended S-parameters with the corresponding conversion to mixed-mode S-parameters.

In this work, we propose a simple strategy to detect mode conversion in balanced structures (potentially subjected to symmetry imbalances), which is then applied to the

Manuscript received Month DD, YYYY; revised Month DD, YYYY; accepted Month DD, YYYY.

This work was supported by MINECO-Spain (project TEC2016-75650-R), by *Generalitat de Catalunya* (project 2017SGR-1159), by *Institució Catalana de Recerca i Estudis Avançats* (who awarded Ferran Martín), and by FEDER funds. J. Muñoz-Enano acknowledges *Secretaria d'Universitats i Recerca* (Gen. Cat.) and *European Social Fund* for the FI grant. Paris Vélez acknowledges the *Juan de la Cierva* Program for supporting him through Project IICI-2017-31339. M. Gil acknowledges the *Universidad Politécnica de Madrid* Young Researchers Support Program (VJIDOCUPM18MGB) for its support.

J. Muñoz-Enano, P. Vélez, and F. Martín are with GEMMA/CIMITEC, Departament d'Enginyeria Electrònica, Universitat Autònoma de Barcelona, 08193 Bellaterra, Spain. E-mail: Ferran.Martin@uab.es.

M. Gil is with Departamento Ingeniería Audiovisual y Comunicaciones, Universidad Politécnica de Madrid, 28031 Madrid, Spain.

J. Mata-Contreras is with Departamento de Ingeniería de Comunicaciones, Universidad de Málaga, 29016 Málaga, Spain.

implementation of differential sensors. This strategy consists of adding a pair of rat-race couplers conveniently connected to the pair of input and output ports of the balanced sensing structure, resulting in a simple two-port device. The main advantage is the simplicity in the measurement of the output variable, the single-ended transmission coefficient of the whole two-port structure, intimately related to the cross-mode transmission coefficient of the balanced sensing part. A detailed analysis of the proposed system, which will provide important hints for sensitivity optimization, is also carried out. This is a relevant contribution of the present work. Moreover, such analysis is validated from full-wave electromagnetic simulations, and then used for the design of a simple differential sensor and comparator, based on a pair of meandered lines (intended to demonstrate/validate the proposed sensing strategy, including sensitivity optimization).

The work is organized as follows. The proposed mode conversion detector and working principle are presented in Section II. The analysis focused on the determination of the transmission coefficient (the key parameter) for the general case of an arbitrary four-port test structure (to account for possible symmetry imbalances, the case of actual interest) is carried out in Section III. Then, Section IV considers the particular case of a pair of uncoupled matched lines, and the conditions for sensitivity optimization (i.e., enhancement of the transmission coefficient with the phase difference of the two lines), are discussed. In Section V, the conclusions of the previous analysis are applied to the design of a differential sensor/comparator, which is experimentally validated in Section VI. Such validation includes a defect detector, a sensor to determine the dielectric constant of low-loss samples, and a sensor to determine the volume fraction of liquid solutions. Finally, the main conclusions of the work are highlighted in Section VII.

II. THE PROPOSED MODE CONVERSION DETECTOR AND WORKING PRINCIPLE

The proposed mode conversion detector consists of a pair of rat-race hybrid couplers connected to the four-port (arbitrary) circuit under study as shown in Fig. 1. Such four-port circuit, not necessarily reciprocal, can be either described by the single-ended S-parameters, or by the mixed-mode S-parameters. According to the port designation (Fig. 1), the single-ended S-parameter matrix is

$$\mathbf{S}_{se} = \begin{pmatrix} S_{AA} & S_{AA'} & S_{AB} & S_{AB'} \\ S_{A'A} & S_{A'A'} & S_{A'B} & S_{A'B'} \\ S_{BA} & S_{BA'} & S_{BB} & S_{BB'} \\ S_{B'A} & S_{B'A'} & S_{B'B} & S_{B'B'} \end{pmatrix} \quad (1)$$

whereas the mixed-mode S-parameter matrix can be expressed as a combination of four order-2 matrices as follows

$$\mathbf{S}_{mm} = \begin{pmatrix} \mathbf{S}^{dd} & \mathbf{S}^{dc} \\ \mathbf{S}^{cd} & \mathbf{S}^{cc} \end{pmatrix} = \begin{pmatrix} S_{11}^{dd} & S_{12}^{dd} & S_{11}^{dc} & S_{12}^{dc} \\ S_{21}^{dd} & S_{22}^{dd} & S_{21}^{dc} & S_{22}^{dc} \\ S_{11}^{cd} & S_{12}^{cd} & S_{11}^{cc} & S_{12}^{cc} \\ S_{21}^{cd} & S_{22}^{cd} & S_{21}^{cc} & S_{22}^{cc} \end{pmatrix} \quad (2)$$

where the mixed mode S-parameters are related to the single-mode S-parameters according to well-known transformations (see, e.g., [2]), i.e.,

$$\mathbf{S}^{dd} = \frac{1}{2} \begin{pmatrix} S_{AA} - S_{AB} - S_{BA} + S_{BB} & S_{AA'} - S_{AB'} - S_{BA'} + S_{BB'} \\ S_{A'A} - S_{A'B} - S_{B'A} + S_{B'B} & S_{A'A'} - S_{A'B'} - S_{B'A'} + S_{B'B'} \end{pmatrix} \quad (3a)$$

$$\mathbf{S}^{cc} = \frac{1}{2} \begin{pmatrix} S_{AA} + S_{AB} + S_{BA} + S_{BB} & S_{AA'} + S_{AB'} + S_{BA'} + S_{BB'} \\ S_{A'A} + S_{A'B} + S_{B'A} + S_{B'B} & S_{A'A'} + S_{A'B'} + S_{B'A'} + S_{B'B'} \end{pmatrix} \quad (3b)$$

$$\mathbf{S}^{dc} = \frac{1}{2} \begin{pmatrix} S_{AA} + S_{AB} - S_{BA} - S_{BB} & S_{AA'} + S_{AB'} - S_{BA'} - S_{BB'} \\ S_{A'A} + S_{A'B} - S_{B'A} - S_{B'B} & S_{A'A'} + S_{A'B'} - S_{B'A'} - S_{B'B'} \end{pmatrix} \quad (3c)$$

$$\mathbf{S}^{cd} = \frac{1}{2} \begin{pmatrix} S_{AA} - S_{AB} + S_{BA} - S_{BB} & S_{AA'} - S_{AB'} + S_{BA'} - S_{BB'} \\ S_{A'A} - S_{A'B} + S_{B'A} - S_{B'B} & S_{A'A'} - S_{A'B'} + S_{B'A'} - S_{B'B'} \end{pmatrix} \quad (3d)$$

Note that the pair of composite differential- and common-mode ports, necessary to derive the above transformations, are considered to be the ports A-B and A'-B' (driven as a pair). Thus, for perfect symmetry conditions, with regard to the indicated bisection plane O-O', the cross-mode (or mode conversion) matrices, \mathbf{S}^{cd} and \mathbf{S}^{dc} , are null. By contrast, in the use of the mode conversion detector as differential sensor or comparator (Section V), a symmetry imbalance will be deliberately generated. Particularly, in such application, the sensitive parts of the structure (symmetrically located with regard to the O-O' plane) are loaded with different samples (the reference sample, REF, and the sample under test, SUT). The result of such imbalance is mode conversion, and, consequently, $\mathbf{S}^{cd} \neq \mathbf{0}$ and $\mathbf{S}^{dc} \neq \mathbf{0}$.

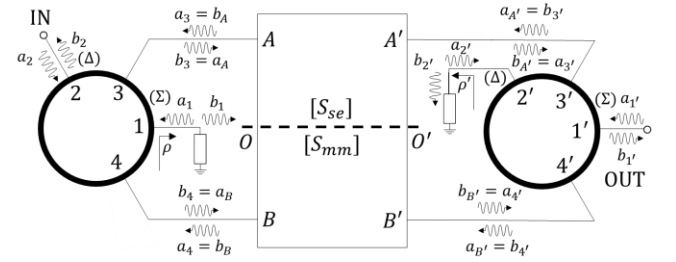


Fig. 1. Structure of the proposed mode conversion detector.

The input port of the two-port mode conversion detector is the Δ -port of the first coupler (port 2), whereas the output port is the Σ -port of the second coupler (port 1'). The ports in both couplers are differentiated by means of a super-index prime ($'$) in the second coupler. For a matched isolated port (Σ -port) in coupler 1 (port 1), such coupler acts as a balun, providing out of phase signals at ports 3 and 4 (i.e., a pure differential signal in the differential port 3-4, or A-B). Similarly, by terminating the Δ -port in the second coupler (port 2') with a matched load, the Σ -port (port 1') only detects common-mode signals, if they are present, at the composite port 3'-4' (or A'-B'). Therefore, the structure is sensitive to differential-mode to common-mode conversion, potentially caused by symmetry imbalances, either undesired or deliberate. In the former case, the structure can be used to detect fabrication inaccuracies in balanced circuits. In the second case (deliberate symmetry truncation), the device is useful as differential sensor (as it has been pointed out), the case of interest in this work.

According to the previous words, it is expected that the transmission coefficient of the complete two-port structure (including the pair of couplers and the four-port network in between) is related to the cross-mode S-parameters of the four-port network, in turn correlated with the level of asymmetry of such network. The calculation of such

transmission coefficient is carried out in the next section, where the general case of ports 1 and 2' terminated with arbitrary loads is considered.

III. GENERAL ANALYSIS

The working principle of the proposed mode conversion detector has been explained by considering the isolated ports of the couplers (ports 1 and 2') terminated with matched loads. However, it does not mean that this termination is the optimum one in order to obtain a maximum variation of the modulus of the transmission coefficient of the structure as symmetry imbalances increase (sensitivity optimization). Therefore, the following analysis, devoted to obtain the transmission coefficient of the mode conversion detector, is carried out by considering arbitrary loads in ports 1 and 2', described by reflection coefficients ρ and ρ' , respectively (see Fig. 1). Let us call f_0 the operating frequency of the device, at which the length of the ring couplers is exactly 1.5λ (λ being the guided wavelength), and let Z_0 be the reference impedance of the ports. With the port designation of Fig. 1, the S-parameter matrix of the couplers (at f_0) is [88]

$$\mathbf{S} = \mathbf{S}' = -\frac{j}{\sqrt{2}} \begin{pmatrix} 0 & 0 & 1 & 1 \\ 0 & 0 & 1 & -1 \\ 1 & 1 & 0 & 0 \\ 1 & -1 & 0 & 0 \end{pmatrix} \quad (4)$$

In the present analysis, we will deal with the normalized amplitudes of the voltage waves incident to (a_i) or reflected from (b_i) the ports, where the sub-index i identifies the port. The variable of interest in this study, the transmission coefficient of the whole structure, is given by

$$S_{1'2} = \left. \frac{b_1'}{a_2} \right|_{a_1=0} \quad (5)$$

where, again, the super index prime is used to distinguish between the normalized amplitudes of the incident and reflected waves in both couplers. According to (4), b_1' is

$$b_1' = -\frac{j}{\sqrt{2}}(a_3' + a_4') \quad (6)$$

where the normalized amplitude of the incident voltages at ports 3' and 4' can be expressed as a function of the elements of the single-ended S-parameter matrix of the four-port network, i.e.,

$$a_3' = S_{A'A}b_3 + S_{A'A'}b_3' + S_{A'B}b_4 + S_{A'B'}b_4' \quad (7a)$$

$$a_4' = S_{B'A}b_3 + S_{B'A'}b_3' + S_{B'B}b_4 + S_{B'B'}b_4' \quad (7b)$$

Note that (7) results from the following (trivial) correspondence between normalized amplitudes of incident and reflected voltages waves of the couplers (right side members) and the four-port network (left side members):

$$a_A = b_3 \quad (8a)$$

$$b_A = a_3 \quad (8b)$$

$$a_{A'} = b_3' \quad (8c)$$

$$b_{A'} = a_3' \quad (8d)$$

$$a_B = b_4 \quad (8e)$$

$$b_B = a_4 \quad (8f)$$

$$a_{B'} = b_4' \quad (8g)$$

$$b_{B'} = a_4' \quad (8h)$$

The normalized amplitudes of the reflected voltage waves (referred to the couplers) that appear in the right-hand side members in (7) are given by:

$$b_3 = -\frac{j}{\sqrt{2}}(a_1 + a_2) = -\frac{j}{\sqrt{2}}(\rho b_1 + a_2) \quad (9a)$$

$$b_3' = -\frac{j}{\sqrt{2}}(a_1' + a_2') = -\frac{j}{\sqrt{2}}\rho' b_2' \quad (9b)$$

$$b_4 = -\frac{j}{\sqrt{2}}(a_1 - a_2) = -\frac{j}{\sqrt{2}}(\rho b_1 - a_2) \quad (9c)$$

$$b_4' = -\frac{j}{\sqrt{2}}(a_1' - a_2') = -\frac{j}{\sqrt{2}}(-\rho' b_2') \quad (9d)$$

with $a_1 = \rho b_1$ and $a_2' = \rho' b_2'$. Note also that $a_1' = 0$ in (9), since port 1' should be matched for the calculation of the transmission coefficient (see expression 5). By introducing the right-hand side terms of (9) in (7), and the resulting expressions in (6), the normalized amplitude of the output voltage wave at port 1' is found to be:

$$b_1' = -\{S_{21}^{cc}\rho b_1 + S_{21}^{cd}a_2 + S_{22}^{cd}\rho' b_2'\} \quad (10)$$

where the correspondence between mixed-mode and single-ended S-parameters of the four-port network (expressions 3) has been used.

In order to obtain the transmission coefficient of the whole structure according to (5), the first and third terms of the second member in (10) must be written as a function of a_2 . For that purpose, the first step is to express b_1 and b_2' , given by

$$b_1 = -\frac{j}{\sqrt{2}}(a_3 + a_4) \quad (11a)$$

$$b_2' = -\frac{j}{\sqrt{2}}(a_3' - a_4') \quad (11b)$$

in terms of the same variables that appear in the second member of (10). The procedure is very similar to the one detailed before to obtain equation (10), and for that reason it is not repeated. The obtained results are found to be:

$$b_1 = -\{S_{11}^{cc}\rho b_1 + S_{11}^{cd}a_2 + S_{12}^{cd}\rho' b_2'\} \quad (12)$$

$$b_2' = -\{S_{21}^{dc}\rho b_1 + S_{21}^{dd}a_2 + S_{22}^{dd}\rho' b_2'\} \quad (13)$$

where, again, (3) has been used. From (12), b_1 can be expressed in terms of a_2 and b_2' , i.e.,

$$b_1 = -\frac{S_{11}^{cd}a_2 + S_{12}^{cd}\rho' b_2'}{1 + S_{11}^{cc}\rho} \quad (14)$$

By introducing (14) in (13), b_2' can be isolated and expressed in terms of a_2 as follows

$$b_2' = M' \cdot a_2 \quad (15)$$

where M' , introduced to simplify the notation, depends only on the mixed-mode S parameters of the four-port network, as well as on the reflection coefficients of the loads present at ports 1 and 2', i.e.,

$$M' = -\frac{S_{21}^{dd} - \rho S_{21}^{dc} S_{11}^{cd}}{1 + \rho S_{11}^{cc}} \quad (16)$$

From (14), b_1 can be expressed in terms of a_2 as

$$b_1 = M a_2 \quad (17)$$

where

$$M = -\frac{S_{11}^{cd} + \rho' M' S_{12}^{cd}}{1 + \rho S_{11}^{cc}} \quad (18)$$

Finally, by introducing (15) and (17) in (10), b'_1 can be expressed as proportional to a_2 , and the transmission coefficient, given by (5), is found to be

$$S_{1'2} = -\{S_{21}^{cc}\rho M + S_{21}^{cd} + S_{22}^{cd}\rho' M'\} \quad (19)$$

Inspection of (19) reveals that for perfectly balanced four-port networks (i.e., with $\mathbf{S}^{cd} = \mathbf{S}^{dc} = \mathbf{0}$), $S_{1'2} = 0$, as expected (note that $M = 0$ for balanced structures). A detailed analysis of (19) indicates that for unbalanced four-port networks, $S_{1'2}$ can be also null. However, this occurs for very specific combinations of port loading (i.e., ρ and ρ') and mixed-mode S-parameters of the four-port network [89]. Thus, when symmetry is truncated, in general $S_{1'2}$ is not zero. Hence, the structure can be used as a detector able to determine the level of asymmetry in a four-port network (mode conversion detector).

Interestingly, for matched terminations at ports 1 and 2' ($\rho = \rho' = 0$), the transmission coefficient of the mode conversion detector is found to be

$$S_{1'2} = -S_{21}^{cd} \quad (20)$$

which coincides with the cross-mode transmission coefficient of the four-port network (except the sign). Thus, the proposed structure provides a straightforward way to obtain the cross-mode transmission coefficient in four-port networks. Note, however, that M and M' depend on various elements of the cross-mode matrices. Therefore, it is not a priori clear that the preferred option for sensitivity optimization is to terminate ports 1 and 2' with matched loads. To determine the convenient terminations at those ports (for sensitivity enhancement), the mixed-mode (or single-ended) S-parameters of the four-port network must be known. Nevertheless, from the point of view of fabrication simplicity and cost, terminating the ports with open-circuits ($\rho = \rho' = 1$) is equivalent to eliminate one port of each coupler, thereby avoiding the connection of surface mount devices (SMD), as required for matched terminations or for arbitrary loads, or vias (corresponding to short-circuit terminations, i.e., $\rho = \rho' = -1$).

A case of special interest is the one corresponding to a pair of matched and uncoupled lines, to be discussed in the next section, and then applied to the implementation of a differential sensor and comparator.

IV. ANALYSIS RESULTS FOR MATCHED AND UNCOUPLED LINES AND SENSITIVITY OPTIMIZATION

For a four-port network consisting of a pair of matched and uncoupled lines (Fig. 2), the mixed-mode S-parameters that explicitly appear in (19) are

$$S_{22}^{cd} = 0 \quad (21a)$$

$$S_{21}^{cd} = \frac{1}{2}(e^{-j\phi_A} - e^{-j\phi_B}) \quad (21b)$$

$$S_{21}^{cc} = \frac{1}{2}(e^{-j\phi_A} + e^{-j\phi_B}) \quad (21c)$$

where ϕ_A and ϕ_B are the electrical lengths of the lines between ports A-A' (line A) and B-B' (line B),

respectively. The other term needed for the determination of $S_{1'2}$ is M , given by

$$M = \frac{\rho'}{4}(e^{-j\phi_A} - e^{-j\phi_B}) \left\{ \frac{e^{-j\phi_A} + e^{-j\phi_B}}{1 - \frac{\rho\rho'}{4}(e^{-j\phi_A} - e^{-j\phi_B})^2} \right\} \quad (22)$$

and the transmission coefficient (19) is found to be

$$S_{1'2} = -\frac{1}{2}(e^{-j\phi_A} - e^{-j\phi_B}) \left\{ 1 + \frac{\rho\rho'}{4} \frac{(e^{-j\phi_A} + e^{-j\phi_B})^2}{1 - \frac{\rho\rho'}{4}(e^{-j\phi_A} - e^{-j\phi_B})^2} \right\} \quad (23)$$

Note that expression (23) has been obtained by neglecting losses. This approximation is justified as far as the considered substrate (for device implementation) is a low-loss microwave substrate, and provided the imbalances (if they are present) are caused by dielectric loading of the lines (the REF and SUT samples in lines A and B, respectively) with low-loss materials. Nevertheless, the generalization of (23) by considering the lines loaded with lossy materials (e.g., liquids) is carried out in Appendix A.

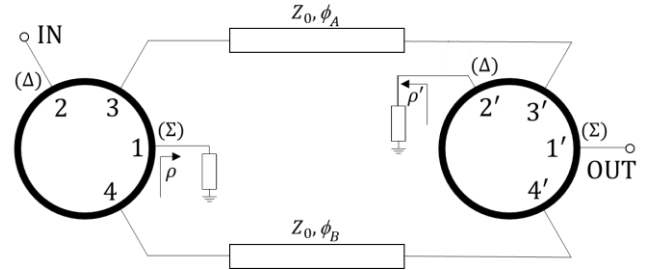


Fig. 2. Mode conversion detector applied to a pair of matched and uncoupled lines.

Let us now designate the first and second term of the right-hand side member of (23) as P and Q , respectively. The modulus of (23), the variable of interest for the use of the considered structure for sensing purposes, is given by the modulus of P , i.e.,

$$|P| = \left| \sin\left(\frac{\phi_A - \phi_B}{2}\right) \right| \quad (24)$$

times the modulus of Q . This later quantity cannot be expressed in a straightforward form. However, for small asymmetries (imbalances), corresponding to similar (but not identical) values of the electrical lengths of both lines ($\phi_A \approx \phi_B$), the modulus of the transmission coefficient can be approximated by

$$|S_{1'2}| \approx \left| \frac{\phi_A - \phi_B}{2} \right| \cdot \left| 1 + \rho\rho' e^{-j(\phi_A + \phi_B)} \right| \quad (25)$$

The case of small imbalances is justified since the detection of tiny differences between the phases of both lines (e.g., caused by slightly different sample loading in the lines) is of interest for high sensitive detectors and sensors, as it will be discussed in the next section.

In view of (25), it follows that for small asymmetries, termination of any of the isolated ports (1 or 2') with a matched load (i.e., $\rho\rho' = 0$) is a sufficient condition to obtain a proportional dependence of the modulus of the transmission coefficient with the phase difference. Thus, by considering the phase difference, $\Delta\phi = \phi_A - \phi_B$, as the input variable, the sensitivity for small perturbations is constant and given by

$$S = \frac{\partial |S_{1'2}|}{\partial (\Delta\phi)} = \frac{1}{2} \quad (26)$$

For $\rho \cdot \rho' \neq 0$, the sensitivity (as defined above) for small perturbations is not constant, but it can be either enhanced or degraded, depending on the phase of the lines ($\phi_A \approx \phi_B$).

Let us now consider two canonical cases: (i) $\rho \cdot \rho' = 1$ (corresponding, e.g., to $\rho = \rho' = \pm 1$, and (ii) $\rho \cdot \rho' = -1$ (corresponding, e.g., to $\rho = 1$ and $\rho' = -1$, or to $\rho = -1$ and $\rho' = 1$). In the former case, $|Q| \approx 0$ if $\phi_A \approx \phi_B \approx (2n+1)\pi/2$ (with $n = 0, 1, 2, 3, \dots$), and $|Q| \approx 2$ if $\phi_A \approx \phi_B \approx n\pi$. Thus, if ports 1 and 2' are left open ($\rho = \rho' = 1$) or grounded ($\rho = \rho' = -1$), sensitivity is optimized when the length of the pair of matched and uncoupled lines is roughly a half wavelength (or a multiple of this length). In this case, the sensitivity in the limit of small asymmetries is $S = 1$. Conversely, for $\rho \cdot \rho' = -1$, $|Q| \approx 2$ if $\phi_A \approx \phi_B \approx (2n+1)\pi/2$, and $|Q| \approx 0$ if $\phi_A \approx \phi_B \approx n\pi$. Thus, if one port is left open and the other one is short-circuited to ground, the optimum line length for sensitivity optimization (with $S = 1$, as well) is an odd multiple of a quarter wavelength.

It should be mentioned that such canonical cases can be also obtained by means of purely reactive loads. For instance, case (i) results by considering, e.g., $\rho = j$ (pure inductance) and $\rho' = -j$ (pure capacitance). Nevertheless, the most interesting case from a practical viewpoint is case (i) with $\rho = \rho' = 1$, since neither a specific load nor a via is required in the isolated ports (1 and 2') of the couplers.

For the validation of the previous sensitivity analysis, we have represented the exact value of the term Q [in brackets in expression (23)] (Fig. 3). Such term can be rewritten as

$$Q = \frac{1}{1 - \frac{\rho \rho' [\cos(\phi_A - \phi_B) + 1]}{2[\rho \rho' + j \sin(\phi_A + \phi_B) + \cos(\phi_A + \phi_B)]}} \quad (27)$$

It can be seen in Fig. 3 that when $\phi_A \approx \phi_B$, Q approaches 0 or 2 for the phase conditions indicated above, depending on the specific case ($\rho \cdot \rho' = 1$ or $\rho \cdot \rho' = -1$).

Figure 4 depicts the exact value of the transmission coefficient (expression 23), as well as the sensitivity, as a function of the phase difference between the lines ($\Delta\phi = \phi_A - \phi_B$) by considering the phase of line A set to a fixed value of $\phi_A = \pi/2$ [Fig. 4(a)] and $\phi_A = \pi$ [Fig. 4(b)]. For small values of $\Delta\phi$, the sensitivity is optimized for $\rho \cdot \rho' = 1$ and $\phi_A = \pi$ (or $n\pi$), or for $\rho \cdot \rho' = -1$ and $\phi_A = \pi/2$ [or $(2n+1)\pi/2$], in agreement to the previous analysis based on the approximate expression (25). Indeed, we have also inferred the transmission coefficient and the sensitivity that results from (25), valid for small perturbations, and we have depicted it in Fig. 4. The agreement is progressively better as $\Delta\phi$ tends to zero, as expected. Figure 4 also depicts the transmission coefficient and sensitivity corresponding to $\rho \cdot \rho' = 0$. In this case, the sensitivity varies with $\Delta\phi$, being roughly constant for small perturbations ($\Delta\phi \approx 0$), but it does not depend on the phase of line A.

According to these results, a differential sensor and comparator based on a pair of matched and uncoupled lines with the phases set to 2π , and with open-ended loads at ports 1 and 2' ($\rho = \rho' = 1$) has been designed and fabricated for validation purposes (to be discussed in the next section).

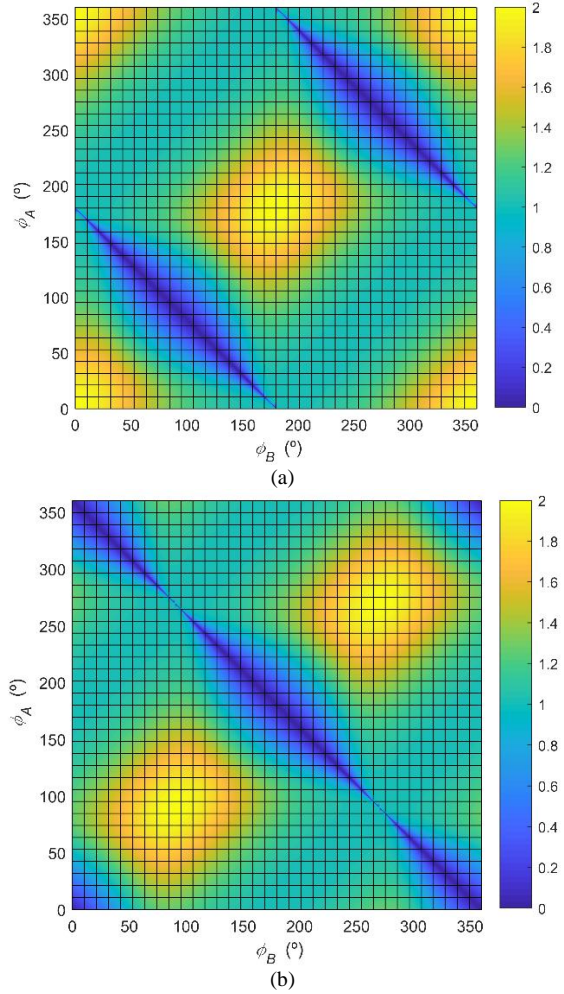


Fig. 3. Variation of the term Q as a function of the electrical lengths of line A (ϕ_A) and line B (ϕ_B). (a) Q for $\rho \cdot \rho' = 1$; (b) Q for $\rho \cdot \rho' = -1$.

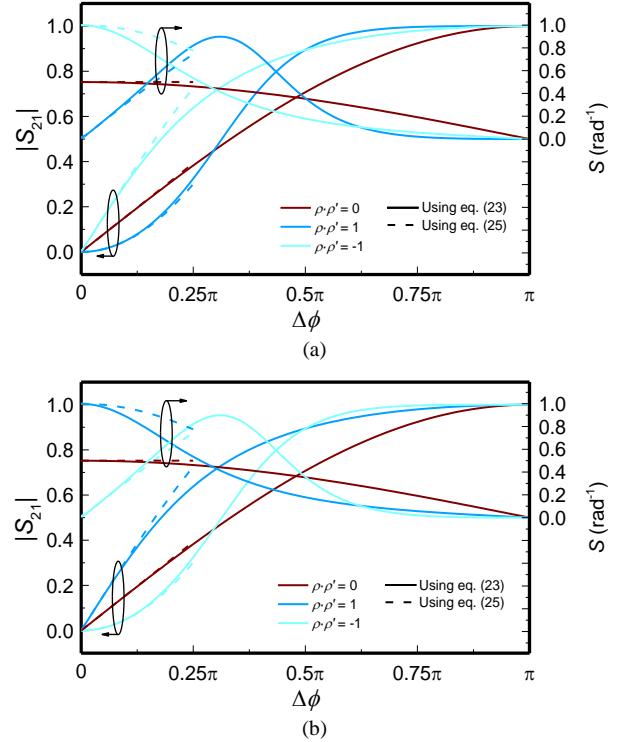


Fig. 4. Variation of the transmission coefficient and the sensitivity as a function of the phase difference ($\Delta\phi = \phi_A - \phi_B$) by considering the electrical length of line A (ϕ_A) set to a fixed value. (a) $\phi_A = \pi/2$; (b) $\phi_A = \pi$. For comparison purposes, the transmission coefficient and the sensitivity that results when $\rho \cdot \rho' = 0$ is also included in the figures.

V. SENSOR/COMPARATOR DESIGN AND FABRICATION

The analysis of the previous section has been used to design the proposed sensor/comparator. The operating frequency has been set to $f_0 = 2$ GHz, and the considered substrate for sensor fabrication is the *Rogers RO4003C* with dielectric constant $\epsilon_r = 3.55$, thickness $h = 0.8128$ mm and dissipation factor $\tan\delta = 0.0021$. With these substrate parameters and frequency, the dimensions of the rat-race hybrid couplers are those indicated in Fig. 5, where the whole sensor is depicted (the width of the ring lines is the one corresponding to a characteristic impedance of 70.71Ω). Identical meandered lines with $50\text{-}\Omega$ impedance and length of 84.93 mm complete the sensing structure. This line length corresponds to an electrical length of 2π at f_0 , provided the sensing regions (indicated in Fig. 5 with dashed rectangles) are covered by a piece of non-metalized *Rogers RO3010* substrate with dielectric constant $\epsilon_r = 10.2$, thickness $h = 1.27$ mm and dissipation factor $\tan\delta = 0.0022$, the reference (REF) sample in our study. With this electrical length of the lines, the sensitivity is optimized (see section IV), provided $\rho\rho' = 1$ (note that the isolated ports of both couplers are opened, and thereby $\rho = \rho' = 1$). It should be mentioned that the characteristic impedance of the line varies slightly in the sensing region, due to the presence of the REF sample. Nevertheless, the conclusions relative to the previous analysis prevail, as it will be shown later.

The device has been fabricated by means of a *LPKF H100* drilling machine. The simulated and measured responses of the device without any material in the sensing regions, inferred by means of the *Keysight Momentum* commercial software and through the *Agilent N5221A PNA* vector network analyzer, respectively, are depicted in Fig. 6. The measured transmission coefficient at f_0 is smaller than -60 dB, indicating that the fabricated structure exhibits good balance between the meandered lines. This is an essential aspect with direct impact on sensor/comparator resolution. The measured response that results by loading both lines with the REF sample indicated before is also included in Fig. 6. The response exhibits an insertion loss of -60 dB at f_0 , pointing out that line balance is maintained by loading the lines with identical samples (to minimize the effects of the air gap, the samples have been attached to the lines by means of screws).

In order to validate the sensitivity analysis of Section IV, we have obtained the simulated transmission coefficient at f_0 by considering the REF line loaded with the REF sample, and the other line loaded with a hypothetical material of identical dimensions and different dielectric constants (the loss tangent being identical). Figure 7(a) depicts the modulus of the transmission coefficient at f_0 , as a function of the variation of the dielectric constant of the sample under test (SUT), where such variation is expressed as percentage with regard to the nominal value of the REF sample (with dielectric constant $\epsilon_r = 10.2$). As it can be seen in the figure, the output variable exhibits a roughly linear variation with the differential dielectric constant, and the average sensitivity with this variable has been found to be $S = \partial|S_{21}|/\partial \% \epsilon_r = 0.0052$.

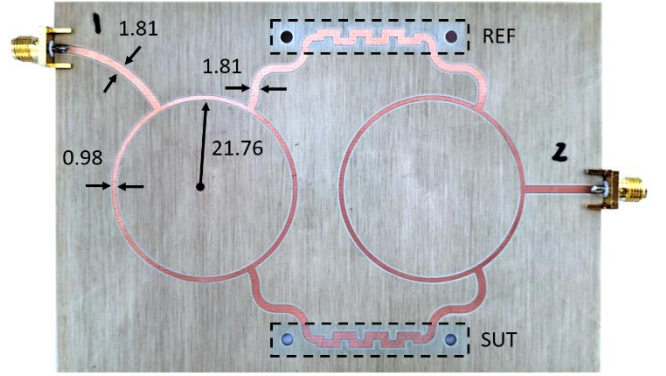


Fig. 5. Photograph of the fabricated sensor/comparator. Dimensions are given in mm (millimeters).

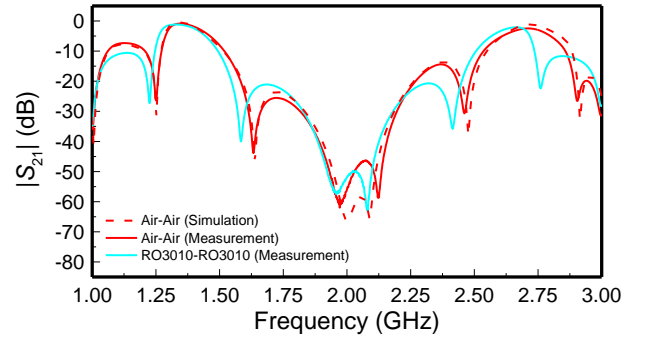


Fig. 6. Frequency response (measured and simulated) of the fabricated sensor/comparator without line loading, and measured frequency response with the sensing region loaded with the REF sample in both lines.

From independent simulations, corresponding to line B with the different SUTs, we have inferred the phase of such line for each case, and we have evaluated expression (23), as well as the output variable that results from the low-perturbation approximation (expression 25). Note that the phase of line A does not vary and corresponds to the optimum case for sensitivity optimization (with $\rho\rho' = 1$, as indicated before). The agreement between the simulated value of the transmission coefficient and the value inferred from (23) is good. The curve corresponding to the approximate expression (25) is undistinguishable from the one of (23) because the phase difference between the lines is small, even for the larger variation of the dielectric constant (20%). This points out the validity of the considered approximation (25), at least up to moderate variations in the differential dielectric constant.

We have repeated the previous simulations by considering an identical structure but elongating the lines, so that the electrical length that results by loading them with the REF sample is 2.5π , corresponding to the worst case in terms of sensitivity (with $Q = 0$). The variation of the transmission coefficient with the differential dielectric constant for this second case is also included in Fig. 7(a). As it can be seen, the variation of the transmission coefficient for small values of the differential dielectric constant is roughly negligible, in agreement with a negligible value of the sensitivity for small perturbations.

In Fig. 7(b), we have depicted the dependence of the transmission coefficient with the simulated differential phase for the two considered cases in Fig. 7(a). For the optimum case (electrical length of the lines of 2π), the average slope has been found to be 0.9762 , corresponding to an average sensitivity with the differential phase very close to the theoretical value ($S = 1$).

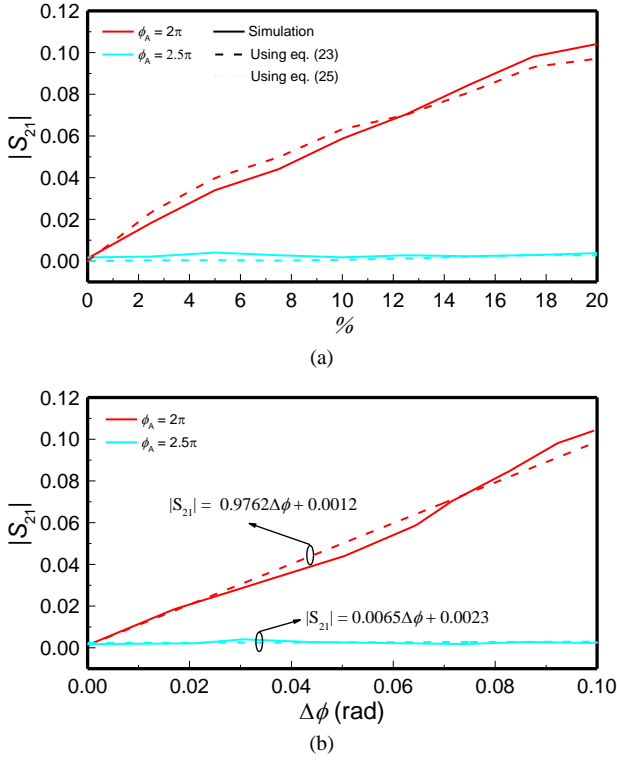


Fig. 7. (a) Simulated transmission coefficient at f_0 , inferred by loading the REF line (A) with the REF sample and line B with SUT samples of different dielectric constant, expressed as percentage variation with regard to the dielectric constant of the REF sample. (b) Representation of the transmission coefficient at f_0 as a function of the differential phase inferred from the simulations. The transmission coefficient that results by evaluating (23) and (25) with the phases of line B inferred from electromagnetic simulation is also included in (a).

The previous simulations validate the analysis of Section IV relative to the dependence of the sensitivity with the length of the lines and with the termination of the isolated ports of the couplers. The slight discrepancies between the simulations and the exact expression providing the output variable, $|S_{21}|$, are due to the fact that the lines are not perfectly matched, as discussed before.

It should be pointed out that the sensitivity of the output variable with the differential dielectric constant increases as the length of the line increases. The reason is that the differential phase is proportional to the length l of the lines, according to

$$\phi_A - \phi_B = (\beta_A - \beta_B)l = \left(\sqrt{\epsilon_{eff,A}} - \sqrt{\epsilon_{eff,B}} \right) \frac{2\pi f_0 l}{c} \quad (28)$$

and, obviously, the effects of the differential dielectric constant on the differential phase are more pronounced as l increases. For this reason, we have designed the sensor with relatively long lines (nevertheless, a tradeoff is necessary in order to avoid an excessively large sensor). In (28), c is the speed of light in vacuum, and $\epsilon_{eff,A}$ and $\epsilon_{eff,B}$ are the effective dielectric constants of line A and B, related to the dielectric constants of the REF and SUT samples, respectively.

VI. EXPERIMENTAL VALIDATION

A. Comparator Functionality

The functionality of the structure as comparator has been carried out by loading line A, the REF line, with the REF sample, and line B subsequently with eight identical samples, but with arrays of drilled holes of different densities. The measured transmission coefficient

corresponding to the different SUT samples are depicted in Fig. 8, where it can be appreciated the significant variation of the transmission coefficient at the operating frequency, f_0 , as the density of holes varies. The comparator is able to detect tiny differences between the REF and SUT samples, as derived from the different transmission coefficient that results when line B is loaded with the REF sample and with the SUT with the smaller density of holes (the photograph of the eight fabricated SUTs is shown in Fig. 9).

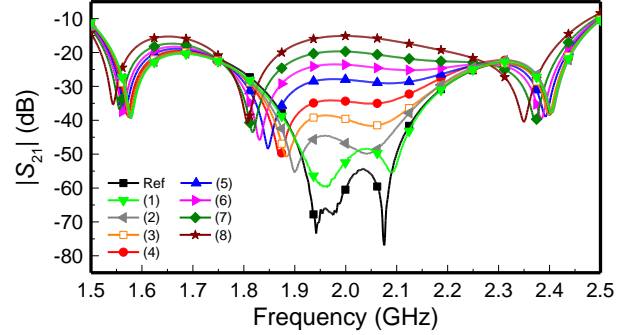


Fig. 8. Measured transmission coefficient that results by loading line A with the REF sample and line B with the SUT samples depicted in Fig. 9.

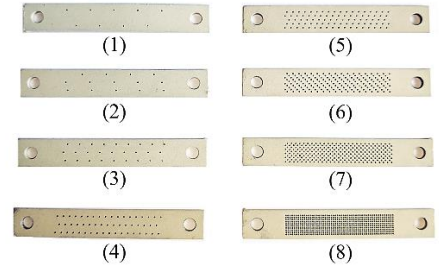


Fig. 9. Photograph of the SUT samples obtained by drilling hole arrays of different densities in samples identical to the REF sample.

B. Dielectric Constant Measurements

We have also loaded line B with different samples with well-known dielectric constant, particularly different types of un-cladded dielectric substrates (i.e., *FR4* with $\epsilon_r = 4.6$ and *RO4003C* with $\epsilon_r = 3.55$). The measured responses of the sensor that result by loading line B with such SUT samples and line A with the REF sample, are depicted in Fig. 10. The transmission coefficients at f_0 are depicted in Fig. 11, from which we have obtained the calibration curve, also depicted in the figure. From this curve, the dielectric constant of the SUT can be inferred by measuring the corresponding transmission coefficient. Note that such curve is useful for the dielectric characterization of materials with dielectric constant smaller than the one of the REF sample, with $\epsilon_r = 10.2$. Moreover, it is necessary that the thickness of the SUT is comparable to the one of the REF samples and SUTs used for calibration. Nevertheless, if the REF sample and the SUTs are thick enough, such that the electric field lines generated by the lines do not reach the interface between the sample and air, the response of the sensor does not depend on sample thickness.

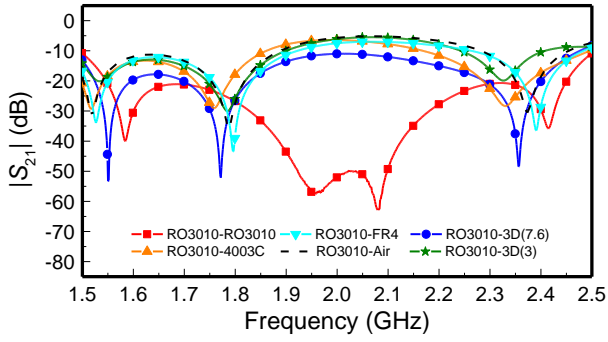


Fig. 10. Measured transmission coefficient that results by loading line A with the REF sample and line B with SUT samples corresponding to the indicated materials.

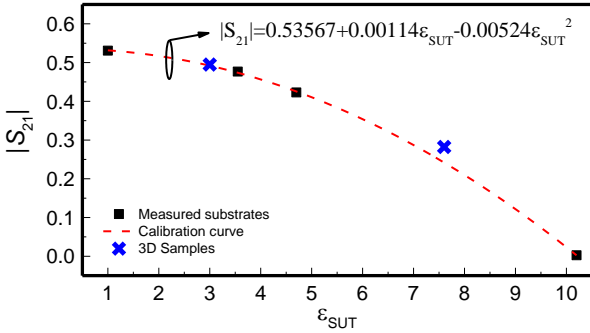


Fig. 11. Transmission coefficient at f_0 corresponding to the SUT samples of Fig. 10.

We have fabricated a pair of SUT samples by means of a 3D printer (*Ultimaker 3 Extended*). The measured dielectric constants, inferred by means of a commercial resonant cavity (*Agilent 85072A*), have been found to be 3 for *PLA* and 7.6 for *RS Pro MT-COPPER* material, respectively. Such samples have the same thickness to the one of the REF sample and to those of the samples used for sensor calibration. The measured transmission coefficients corresponding to such samples are also included in Fig. 10 and Fig. 11, and are in close proximity to the calibration curve, which means that the proposed sensor provides a good estimation of the dielectric constant of the SUT samples. The calibration curve taken from the measured substrates (excluding the 3D-printed SUT samples) for the determination of the dielectric constant is included in Fig. 11. The resulting correlation factor has been found to be $R^2 = 0.9998$. The maximum sensitivity, inferred from the calibration curve, has been found to be $|S| = 0.097$, and the maximum sensitivity, in dB, as derived from the results of Fig. 10 at f_0 is 17.62 dB.

In order to discern if the dielectric constant of the SUT is larger or smaller than the one of the REF sample, let us consider again that the phase variation of line B does not experience a strong change when it is loaded with the SUT sample. Under these conditions, expression (23) can be approximated by

$$S_{1/2} \approx \frac{1}{2} e^{j(\frac{\pi}{2} - \phi_A)} (\phi_A - \phi_B) (1 + \rho \rho' e^{-j(\phi_A + \phi_B)}) \quad (29)$$

For $\phi_A = \pi$ and $\phi_A \approx \phi_B$, the last term in (29) is roughly $Q \approx 2$, as discussed before, and the transmission coefficient can be expressed as

$$S_{1/2} \approx -j(\phi_A - \phi_B) \quad (30)$$

According to (30), the phase of the transmission coefficient is $+90^\circ$ for $\phi_A < \phi_B$ (corresponding to a smaller dielectric constant for the REF sample), and -90° for $\phi_A > \phi_B$ (with a larger dielectric constant for the REF sample). Hence, the phase of the transmission coefficient at f_0 allows us to distinguish whether the dielectric constant of the SUT is larger or smaller than the one of the REF sample, if it is needed.

It should be mentioned that the proposed sensor is useful to measure the dielectric constant of the SUT (subjected to the required thickness, i.e., identical to the one of the REF sample, as indicated before). In the considered samples, the loss tangent is small or moderately small, so that the low-loss approximation holds (and therefore the analysis of Section IV can be adopted). The proposed system is not as sensitive to the effects of losses (in the SUT sample) as resonant methods are [90]-[94]. This means that the system is not appropriate for the measurement of the loss tangent of the SUT sample, and for this reason the measurement of this material parameter is not considered in the present work. Nevertheless, it does not mean that differential sensing involving lossy materials, e.g., liquids, is not possible. On the contrary, the proposed sensor is very appropriate to measure the volume fraction of solute in diluted liquid solutions, to be discussed next. Since liquids, are lossy materials, line imbalance may be caused not only by variations in the dielectric constant between the REF and SUT sample, but also by changes in the loss tangent. For this reason, the generalization of the formulation of Section IV for the lossy case is considered in Appendix A. From this appendix, it is concluded that the same phase conditions for the lines resulting for the lossless case should be applied for sensitivity optimization.

C. Solute Concentration Measurements in Liquid Solutions

In the last campaign of experiments, we have demonstrated the potential of the sensor for the determination of volume fraction in liquid solutions. In particular, we have considered mixtures of isopropanol in deionized (DI) water. In order to determine small volume fractions of isopropanol, the natural REF liquid should be DI water. Moreover, for sensitivity optimization, the sensor, particularly the length of the meandered sensing lines, should be re-dimensioned, so that the electrical length of the REF line (line A) is $\phi_A \approx n\pi$, when such line is loaded with the REF liquid. This has provided a total line length of 131.77 mm, corresponding to $n = 3$, i.e., 46.84 mm longer than the one of the previous device.

For the determination of the volume fraction of different solutions, we have equipped the sensing regions of lines A and B with microfluidic channels. Such channels and the necessary accessories for liquid injection (through syringes) are described in [80]. It should be mentioned that in order to avoid liquid absorption by the substrate, it has been protected by a dry film with thickness 50 μm and dielectric constant 3.56 (see Fig. 12). The presence of such film does not substantially modify the electrical characteristics of the lines. The photograph of the sensor, with the channel and other mechanical parts, including the capillaries for liquid injection, is depicted in Fig. 12.

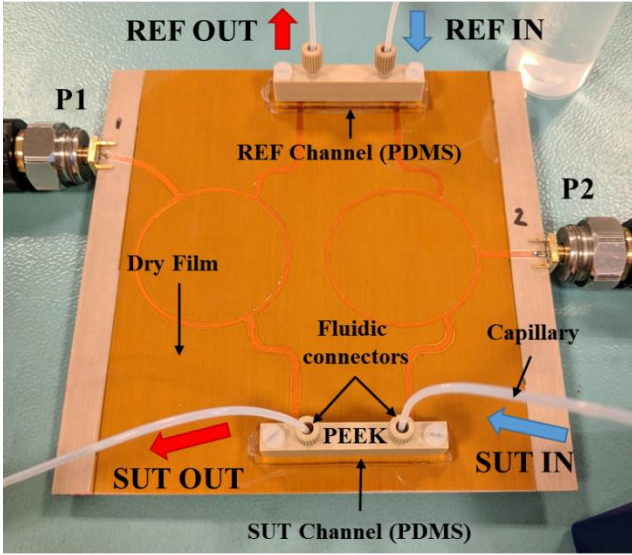


Fig. 12. Photograph of the sensor equipped with fluidic channels.

After adapting the sensor for liquid characterization, we have injected the REF liquid in the REF channel of line A, and subsequently different mixtures of isopropanol in DI water in the SUT channel (line B), starting with a null volume fraction (corresponding to the REF liquid), and progressively increasing the volume fraction of isopropanol. The responses for the different mixtures are depicted in Fig. 13, where it can be seen that the sensor is able to detect small concentrations of isopropanol in DI water. Particularly, a volume fraction as small as 1% of isopropanol can be resolved.

The dependence of the transmission coefficient at f_0 as a function of the isopropanol content is depicted in Fig. 14. The calibration curve, useful for the determination of the volume fraction (F_v) of solute in unknown mixtures of isopropanol and DI water, is also depicted in the figure. Such curve, with a correlation factor of $R^2 = 0.9992$, is

$$F_v(\%) = 154.105 - 18.012e^{-\frac{(S_{21}(dB)+0.0803)}{1.94967}} - 204.76e^{-\frac{(S_{21}(dB)+0.0803)}{580.9732}} \quad (31)$$

By properly modifying sensor dimensions, the sensitivity for different REF liquids could be also optimized (particularly by adjusting the electrical length of the REF line loaded with the REF liquid, so that it satisfies $\phi_A \approx n\pi$). The proposed differential sensor can be of interest, for instance, for monitoring variations of alcohol content in fermentation processes.

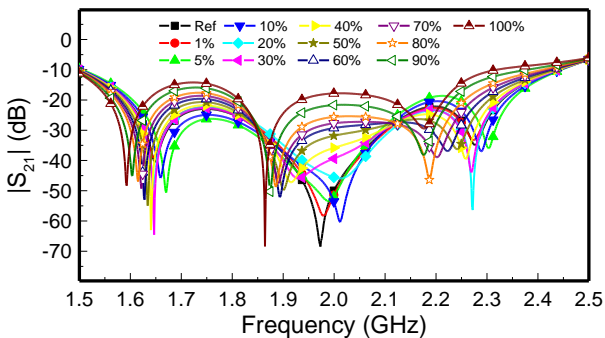


Fig. 13. Measured transmission coefficient that results by loading line A with the REF liquid (DI water) and line B with SUT samples corresponding to the indicated volume fractions of isopropanol in DI water.

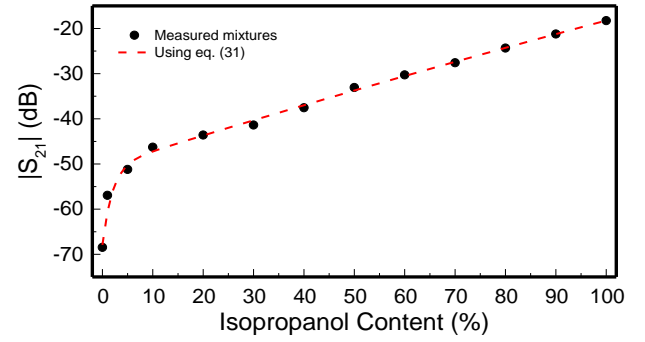


Fig. 14. Value of the transmission coefficient (dB) at f_0 GHz as a function of the isopropanol content.

TABLE I
COMPARISON OF VARIOUS MICROWAVE FLUIDIC SENSORS FOR VOLUME FRACTION MEASUREMENT IN LIQUID SOLUTIONS

Ref.	f_0 (GHz)	F_v (%)
[95]	20	5
[96]	2	10
[97]	1.9	10
[98]	3.5	10
[77]	0.87	10
[99]	1.83	0.005
[79]	0.9	5
[100]	5.3	3.3
[101]	2.3	10
[102]	5.2	20
[103]	1.1	5
This work	1.97	1

In Table I, a comparison of various fluidic sensors devoted to measure the volume fraction of isopropanol, methanol or ethanol is reported. As it can be seen, the proposed sensor is able to resolve 1% of volume fraction. This is a relevant result, only improved by the sensor reported in [99], where a solute concentration as small as 0.005% of volume fraction is detected, although with frequency variations smaller than 1MHz centered around 1.83 GHz.

An advantage of the proposed sensor is that it does not require a wide frequency span for measuring purposes, contrary to most sensors reported in Table I, based on frequency variation or frequency splitting. The sensors reported in [79],[103] (resonant differential sensors) are based on the measurement of the cross mode transmission coefficient. The output variable is indeed the maximum magnitude of the cross mode transmission coefficient, but it occurs at different frequencies (dictated by the SUT). Therefore, a wideband frequency measurement is also required in this case. Despite the fact that the results of Fig. 13 depict the transmission coefficient of the reported sensor in a relatively wide frequency range, the output variable is actually the magnitude of the transmission coefficient at f_0 , the operating frequency. Namely, the sensor operates at a single frequency. This single-frequency operation also applies to the dielectric constant sensor of the previous subsection.

Sensitivity comparison of the reported sensor with other sensors available in the literature is not easy, as far as most sensors are based on frequency variation or frequency splitting. Nevertheless, it is worth mentioning that, as compared to [79],[103] (sensors that use similar working principle) the maximum sensitivity of the reported sensor for the measurement of volume fraction is superior (i.e.,

11.52 dB/%, as compared to 0.70 dB/% in [79] and 0.62 dB/% in [103]). For dielectric constant measurements, the sensitivity of the sensor of the previous subsection (17.62 dB) is by far superior to those of the sensors reported in [79] (0.71 dB) and [103] (0.63 dB).

To end this section, we would like to mention that in the proposed sensor, the considered sensing mechanism is phase variation in the meandered transmission lines. Alternatively, it is possible to consider a sensing region based on a pair of resonator-loaded lines, as in many other differential sensors [79],[80],[103]-[105] not based on a two-port measurement by means of hybrid couplers. In this case, resonator loading modifies the resonance frequency, as well as the peak or notch magnitude (depending on the specific configuration). However, in such potential configuration based on a pair of resonator-loaded lines and a pair of rat-race couplers, mode conversion at the operating frequency of the rat-race couplers is expected to occur, provided the sensing resonators are asymmetrically loaded. Therefore, the proposed mode conversion detector can be also applied in this case. Concerning sensor size, it is mainly dictated by the pair of couplers. Size reduction is possible, obviously, by increasing the operational frequency. Alternatively, the ordinary couplers can be replaced by couplers based on slow-wave artificial lines, with substantially smaller size (see, e.g., [106] and references therein). All these aspects are left for future works.

VII. CONCLUSIONS

In conclusion, a differential sensor and comparator, based on a differential-mode to common-mode conversion detector implemented by means of a pair of rat-race hybrid couplers, has been presented in this paper. The measuring principle of the device is phase variation in a pair of meandered lines. The output variable in such sensor/comparator is the transmission coefficient at the operating frequency, whereas the input variable can be, e.g., the differential dielectric constant (i.e., the one of the sample under test relative to the one of the reference sample), or the volume fraction of solute in a liquid solution. The designed device is also useful to detect tiny differences between the sample under test and the reference sample (comparator functionality). The conditions for sensitivity optimization have been obtained analytically, and from such analysis it has been concluded that the length of the pair of meandered lines (the sensing regions of the device) must be a multiple of a half wavelength, provided the isolated ports of the rat race are left opened (this is a relevant contribution of the paper). The results of the analysis have been corroborated through electromagnetic simulation, by considering sensing structures with different line length. Then, a prototype device has been fabricated and used in different scenarios, including the detection of defects (emulated by drilling hole arrays of different densities in dielectric samples), the measurement of the dielectric constant of slabs, and the measurement of the volume fraction of solute (isopropanol) in liquid solutions (with DI water as solvent). The proposed approach is useful for the implementation of single frequency differential sensors with very competitive sensitivity and resolution.

APPENDIX A

GENERALIZATION OF THE TRANSMISSION COEFFICIENT BY CONSIDERING LOSSES

By considering lines A and B loaded with lossy materials, e.g., liquids, the low-loss approximation used to obtain (23) is no longer valid. However, expression (23) can be easily generalized by simply replacing $j\phi_A = j\beta_A l$ and $j\phi_B = j\beta_B l$ with $\gamma_A l$ and $\gamma_B l$, respectively, where $\gamma_A = \alpha_A + j\beta_A$ and $\gamma_B = \alpha_B + j\beta_B$ are the complex propagation constant of lines A and B, respectively. In the limit of small asymmetries (imbalances), i.e., $\gamma_A \approx \gamma_B$, P and Q can be expressed as

$$P = -\frac{1}{2} e^{-\gamma_A l} (1 - e^{-(\gamma_B - \gamma_A)l}) \approx -\frac{1}{2} e^{-\gamma_A l} (\gamma_B - \gamma_A)l \quad (\text{A.1})$$

$$Q \approx 1 + \rho\rho' e^{-(\gamma_A + \gamma_B)l} \quad (\text{A.2})$$

The modulus of the transmission coefficient is thus given by

$$|S_{1/2}| = |P| \cdot |Q| \quad (\text{A.3})$$

with

$$|P| = \frac{1}{2} e^{-\alpha_A l} \sqrt{(\alpha_B - \alpha_A)^2 l^2 + (\phi_B - \phi_A)^2} \quad (\text{A.4})$$

$$|Q| = |1 + \rho\rho' e^{-(\alpha_A + \alpha_B)l} e^{-j(\phi_A + \phi_B)}| \quad (\text{A.5})$$

Inspection of (A.3)-(A.5) reveals that in order to enhance the sensitivity with either the differential phase (mainly related to the differential dielectric constant) or the differential attenuation constant (mainly dictated by the differential loss tangent), the same phase conditions for the lines resulting for the lossless case (see Section IV), should be applied. Namely, if $\rho\rho' = 1$, it is convenient to choose $\phi_A \approx \phi_B \approx n\pi$. By contrast, for $\rho\rho' = -1$, the phases should satisfy $\phi_A \approx \phi_B \approx (2n+1)\pi/2$. In both cases, the modulus of Q is optimized and given by

$$|Q| = |1 + e^{-(\alpha_A + \alpha_B)l}| \quad (\text{A.6})$$

Note that the resulting $|Q|$ is smaller than 2 (the lossless value), due to the effect of losses. Note also that the optimum sensitivity for small imbalances is no longer $S = 1$ (lossless case), but given by

$$S_{\Delta\phi} = \frac{1}{2} e^{-\alpha_A l} \frac{(\phi_B - \phi_A)}{\sqrt{(\alpha_B - \alpha_A)^2 l^2 + (\phi_B - \phi_A)^2}} |1 + e^{-(\alpha_A + \alpha_B)l}| \quad (\text{A.7})$$

by considering the differential phase as input variable. If the input variable is considered to be the differential attenuation constant, the resulting sensitivity is found to be

$$S_{\Delta\alpha} = \frac{1}{2} e^{-\alpha_A l} \frac{(\alpha_B - \alpha_A)l^2}{\sqrt{(\alpha_B - \alpha_A)^2 l^2 + (\phi_B - \phi_A)^2}} |1 + e^{-(\alpha_A + \alpha_B)l}| \quad (\text{A.8})$$

Inspection of (A.7) indicates that if losses can be neglected ($\alpha_A = \alpha_B = 0$), then the optimum sensitivity satisfies $S_{\Delta\phi} = S = 1$, as expected.

REFERENCES

- [1] W.R. Eisenstadt, B. Stengel, and B.M. Thompson, *Microwave differential circuit design using mixed-mode S-parameters*, Artech House, Norwood, MA, 2006.
- [2] F. Martín, L. Zhu, J. Hong, and F. Medina, *Balanced Microwave Filters*, Wiley-IEEE Press, Hoboken, NJ, 2018.
- [3] B. C. Tseng and L. K. Wu, "Design of miniaturized common-mode filter by multilayer low-temperature co-fired ceramic", *IEEE Trans. Electromagn. Compat.*, vol. 46, no. 4, pp. 571–579, Nov. 2004.

- [4] W. T. Liu, C.-H. Tsai, T.-W. Han, and T.-L. Wu, "An embedded common-mode suppression filter for GHz differential signals using periodic defected ground plane," *IEEE Microw. Wireless Compon. Lett.*, vol. 18, no. 4, pp. 248-250, Apr. 2008.
- [5] S. J. Wu, C. H. Tsai, T. L. Wu, and T. Itoh, "A novel wideband common-mode suppression filter for gigahertz differential signals using coupled patterned ground structure", *IEEE Trans. Microw. Theory Techn.*, vol. 57, no. 4, pp. 848-855, Apr. 2009.
- [6] C.H. Tsai and T.L. Wu, "A broadband and miniaturized common-mode filter for gigahertz differential signals based on negative permittivity metamaterials", *IEEE Trans. Microw. Theory Techn.*, vol. 58, pp. 195-202, Jan. 2010.
- [7] F. de Paulis, L. Raimondo, Sam Connor, B. Archambeault, and A. Orlandi, "Design of a common mode filter by using planar electromagnetic bandgap structures", *IEEE Trans. Adv. Packag.*, vol. 33, no. 4, pp. 994-1002, Nov. 2010.
- [8] J. Naqui, *et al.*, "Split rings-based differential transmission lines with common-mode suppression", *IEEE MTT-S Int. Microwave Symposium*, Baltimore (USA), June 2011.
- [9] J. Naqui, *et al.*, "Common mode suppression in microstrip differential lines by means of complementary split ring resonators: theory and applications", *IEEE Trans. Microw. Theory Techn.*, vol. 60, pp. 3023-3034, Oct. 2012.
- [10] A. Fernandez-Prieto, *et al.*, "Dual-band differential filter using broadband common-mode rejection artificial transmission line", *Prog. Electromagn. Research (PIER)*, vol. 139, pp. 779-797, 2013.
- [11] F.X. Yang, M. Tang, L.S. Wu, and J.F. Mao, "A novel wideband common-mode suppression filter for differential signal transmission", *2014 IEEE Electrical Design of Advanced Packaging & Systems Symposium (EDAPS)*, Bangalore, Dec. 2014, pp. 129-132.
- [12] T.W. Weng, C.H. Tsai, C.H. Chen, D.H. Han, and T.L. Wu, "Synthesis model and design of a common-mode bandstop filter (CM-BSF) with an all-pass characteristic for high-speed differential signals", *IEEE Trans. Microw. Theory Techn.*, vol. 62, no. 8, pp. 1647-1656, Aug. 2014.
- [13] G.H. Shiue, C.M. Hsu, C.L. Yeh, and C.F. Hsu, "A comprehensive investigation of a common-mode filter for gigahertz differential signals using quarter-wavelength resonators", *IEEE Trans. Compon. Packag., Manuf. Technol.*, vol. 4, no. 1, pp. 134-144, Jan. 2014.
- [14] J. H. Choi, P. W. C. Hon, and T. Itoh, "Dispersion analysis and design of planar electromagnetic bandgap ground plane for broadband common-mode suppression", *IEEE Microw. Wireless Compon. Lett.*, vol. 24, no. 11, pp. 772-774, Nov. 2014.
- [15] C.Y. Hsiao, Y.C. Huang, and T.L. Wu, "An ultra-compact common-mode bandstop filter with modified-t circuits in integrated passive device (IPD) process", *IEEE Trans. Microw. Theory Techn.*, vol. 63, no 11, pp. 3624-3631, Nov. 2015.
- [16] A. Fernández-Prieto, *et al.*, "Common-mode suppression for balanced bandpass filters in multilayer liquid crystal polymer technology", *IET Microw. Ant. Propag.*, vol. 9, pp. 1249-1253, Sep. 2015.
- [17] B.-F. Su and T.-G. Ma, "Miniaturized common-mode filter using coupled synthesized lines and mushroom resonators for high-speed differential signals", *IEEE Microw. Wireless Compon. Lett.*, vol. 25, pp.112-114, Feb. 2015.
- [18] Z. Zeng, Y. Yao, and Y. Zhuang, "A wideband common-mode suppression filter with compact-defected ground structure pattern", *IEEE Trans. Electromagn. Compt.*, vol. 57, pp. 1277-1280, Oct. 2015.
- [19] P. Vélez, J. Bonache, and F. Martín, "Differential Microstrip Lines with Common-Mode Suppression based on Electromagnetic Bandgaps (EBGs)", *IEEE Ant. Wireless Propag. Lett.*, vol. 14, pp. 40-43, 2015.
- [20] P. Vélez, *et al.*, "Enhancing common-mode suppression in microstrip differential lines by means of chirped electromagnetic bandgaps (EBGs)", *Microw. Opt. Technol. Lett.*, vol. 58, pp. 328-332, Feb. 2016.
- [21] F. Martin, *et al.*, "The Beauty of Symmetry: Common-Mode Rejection Filters for High-Speed Interconnects and Band Microwave Circuits", *IEEE Microw. Mag.*, vol. 18, no. 1, pp. 42-55, Jan. 2017.
- [22] A. Ebrahimi, T. C. Baum, K. Wang, J. Scott, and K. Ghorbani, "Differential Transmission Lines Loaded With Magnetic LC Resonators and Application in Common Mode Suppression," *IEEE Trans. Circuits Syst. I: Reg. Papers*, vol. 66, pp. 3811 - 3821, Oct. 2019.
- [23] W. Feng, W. Che, and Q. Xue "The proper balance: overview of microstrip wideband balance circuits with wideband common mode suppression", *IEEE Microw. Mag.*, vol. 16, pp. 55-68, Jun. 2015.
- [24] C-H. Wu, C.-H. Wang, and C. H. Chen, "Balanced coupled-resonator bandpass filters using multisection resonators for common-mode suppression and stopband extension", *IEEE Trans. Microw. Theory Techn.*, vol. 55, pp. 1756-1763, Aug. 2007.
- [25] C.-H. Wu, C.-H. Wang, C. H. Chen, "Stopband-extended balanced bandpass filter using coupled stepped-impedance resonators", *IEEE Microw. Wireless Compon. Lett.*, vol. 17, pp. 507-509, Jul. 2007.
- [26] Y. Zhou, H.-W. Deng, Y. Zhao, "Compact balanced-to-balanced microstrip diplexer with high isolation and common-mode suppression," *IEEE Microw. Wireless Compon. Lett.*, vol. 24, pp. 143-144, Mar. 2014.
- [27] A. Fernández-Prieto, A. Lujambio, J. Martel, F. Medina, F. Mesa, and R. R. Boix, "Simple and compact balanced bandpass filters based on magnetically coupled resonators", *IEEE Trans. Microw. Theory Techn.*, vol. 63, pp. 1843-1853, Jun. 2015.
- [28] A. Fernández-Prieto, J. Martel, F. Medina, F. Mesa, R.R. Boix, "Compact balanced FSIR bandpass filter modified for enhancing common-mode suppression", *IEEE Microw. Wireless Compon. Lett.*, vol. 25, pp. 154-156, Mar. 2015.
- [29] A. Fernández-Prieto, J. Bhatker, A. Lujambio, J. Martel, F. Medina, R.R. Boix, "Balanced bandpass filter based on magnetically coupled coplanar waveguide folded-stepped impedance resonators", *Elect. Lett.*, vol. 52, pp. 1229-1231, Jul. 2016.
- [30] T. B. Lim and L. Zhu, "A differential-mode wideband bandpass filter on microstrip line for UWB applications," *IEEE Microw. Wireless Compon. Lett.*, vol. 19, pp. 632-634, Oct. 2009.
- [31] T. B. Lim and L. Zhu, "Highly selective differential-mode wideband bandpass filter for UWB application," *IEEE Microw. Wireless Compon. Lett.*, vol. 21, pp. 133-135, Mar. 2011.
- [32] P. Vélez, *et al.*, "Differential bandpass filter with common mode suppression based on open split ring resonators and open complementary split ring resonators", *IEEE Microw. Wireless Compon. Lett.*, vol. 23, pp. 22-24, Jan. 2013.
- [33] W. Feng, W. Che, Y. Ma, and Q. Xue, "Compact wideband differential bandpass filters using half-wavelength ring resonator", *IEEE Microw. Wireless Compon. Lett.*, vol. 23, pp. 81-83, Feb. 2013.
- [34] P. Vélez, *et al.*, "Differential bandpass filters with common-mode suppression based on stepped impedance resonators (SIRs)", *IEEE MTT-S Int. Microwave Symp.*, June 2013, Seattle (USA).
- [35] A. K. Horestani, M. Durán-Sindreu, J. Naqui, C. Fumeaux, and F. Martín, "S-shaped complementary split ring resonators and application to compact differential bandpass filters with common-mode suppression", *IEEE Microw. Wireless Compon. Lett.*, vol. 24, pp. 150-152, March 2014.
- [36] X.-H. Wang and H. Zhang, "Novel balanced wideband filters using microstrip coupled lines", *Microw. Opt. Technol. Lett.*, vol. 56, pp. 1139-1141, May 2014.
- [37] L. Li, J. Bao, J.-J. Du, and Y.-M. Wang, "Compact differential wideband bandpass filters with wide common-mode suppression", *IEEE Microw. Wireless Compon. Lett.*, vol. 24, no. 3, pp. 164-166, Mar. 2014.
- [38] H. Wang, L.-M. Gao, K.-W. Tam, W. Kang, and W. Wu, "A wideband differential BPF with multiple differential- and common-mode transmission zeros using cross-shaped resonator", *IEEE Microw. Wireless Compon. Lett.*, vol. 24, pp. 854-856, Oct. 2014.
- [39] W. Feng, W. Che, and Q. Xue, "High selectivity wideband differential bandpass filter with wideband common mode suppression using marchand balun", *IEEE Int. Wireless Symp.*, Mar. 2014, Xian (China).
- [40] L. Li, J. Bao, J.-J. Du, and Y.-M. Wang, "Differential wideband bandpass filters with enhanced common-mode suppression using internal coupling technique", *IEEE Microw. Wireless Compon. Lett.*, vol. 24, pp. 300-302, Feb. 2014.
- [41] J. G. Zhou, Y.-C. Chiang, and W. Che, "Compact wideband balanced bandpass filter with high common-mode suppression based on cascade parallel coupled lines" *IET Microw. Ant. Propag.*, vol. 8, pp. 564-570, Jun. 2014.
- [42] P. Velez, J. Selga, M. Sans, J. Bonache, and F. Martin, "Design of differential-mode wideband bandpass filters with wide stop band and common-mode suppression by means of multisection mirrored stepped impedance resonators (SIRs)", *IEEE MTT-S Int. Microwave Symp.*, May 2015, Phoenix, Arizona (USA).
- [43] M. Sans, *et al.*, "Automated design of common-mode suppressed balanced wideband bandpass filters by means of aggressive space mapping (ASM)", *IEEE Trans. Microw. Theory Techn.*, vol. 63, no. 12, pp. 3896-3908, Dec. 2015.
- [44] M. Sans, *et al.*, "Automated design of balanced wideband bandpass filters based on mirrored stepped impedance resonators (SIRs) and interdigital capacitors", *Int. J. Microw. Wireless Technol.*, vol. 8, Issue 4-5, pp. 731-740, Jun. 2016.
- [45] M. Sans, *et al.*, "Optimized wideband differential-mode bandpass filters with broad stopband and common-mode suppression based on

- multi-section stepped impedance resonators and interdigital capacitors”, *IEEE MTT-S Int. Conference on Numerical Electromagnetic and Multiphysics Modeling and Optimization for RF, Microwave and Terahertz Applications (NEMO,17)*, Seville, Spain, May 2017.
- [46] W. Feng and W. Che, “Novel wideband differential bandpass filters based on T-shaped structure”, *IEEE Trans. Microw. Theory. Techn.*, vol. 60, pp. 1560–1568, Jun. 2012.
- [47] X.-H. Wu, Q.-X. Chu, and L.-L. Qiu, “Differential wideband bandpass filter with high-selectivity and common-mode suppression”, *IEEE Microw. Wireless Compon. Lett.*, vol. 2, pp. 644–646, Dec. 2013.
- [48] T. B. Lim and L. Zhu, “Differential-mode ultra-wideband bandpass filter on microstrip line,” *Electron. Lett.*, vol.45, pp. 1124–1125, Oct. 2009.
- [49] X.-H. Wu and Q.-X. Chu, “Compact differential ultra-wideband bandpass filter with common-mode suppression”, *IEEE Microw. Wireless Compon. Lett.*, vol. 22, pp. 456–458, Sep. 2012.
- [50] A. M. Abbosh, “Ultrawideband balanced bandpass filter”, *IEEE Microw. Wireless Compon. Lett.*, vol. 21, pp. 480–482, Sep. 2011.
- [51] H. T. Zhu, W. J. Feng, W. Q. Che, and Q. Xue, “Ultra-wideband differential bandpass filter based on transversal signal-interference concept”, *Electron. Lett.*, vol.47, pp. 1033–1035, Sep. 2011.
- [52] X.-H. Wang, H. Zhang, and B.-Z. Wang, “A novel ultra-wideband differential filter based on microstrip line structures”, *IEEE Microw. Wireless Compon. Lett.*, vol. 23, pp. 128–130, Mar. 2013.
- [53] S. Shi, W.-W. Choi, W. Che, K.-W. Tam, and Q. Xue, “Ultra-wideband differential bandpass filter with narrow notched band and improved common-mode suppression by DGS,” *IEEE Microw. Wireless Compon. Lett.*, vol. 22, pp. 185–187, Apr. 2012.
- [54] C.-H. Lee, C.-I.G. Hsu, and C.-J. Chen, “Band-notched balanced UWB BPF with stepped-impedance slotline multi-mode resonator,” *IEEE Microw. Wireless Compon. Lett.*, vol. 22, pp. 182–184, Apr. 2012.
- [55] J. Shi, C. Shao, J.-X. Chen, Q.-Y. Lu, Y. Peng, and Z.-H. Bao, “Compact low-loss wideband differential bandpass filter with high common-mode suppression”, *IEEE Microw. Wireless Compon. Lett.*, vol. 23, pp. 480–482, Sep. 2013.
- [56] P. Vélez, *et al.*, “Ultra-compact (80mm²) differential-mode ultra-wideband (UWB) bandpass filters with common-mode noise suppression”, *IEEE Trans. Microw. Theory Techn.*, vol. 63, pp. 1272–1280, Apr. 2015.
- [57] M. Sans, *et al.*, “Compact Wideband Balanced Bandpass Filters With Very Broad Common-Mode and Differential-Mode Stopbands”, *IEEE Trans. Microw. Theory Techn.*, vol. 66, no. 2, pp. 737 - 750, Feb. 2018.
- [58] C. Damm, M. Schussler, M. Puentes, H. Maune, M. Maasch, and R. Jakoby, “Artificial transmission lines for high sensitive microwave sensors,” *IEEE Sensors Conf.*, Christchurch, New Zealand, pp.755–758, Oct. 2009.
- [59] C. Damm, *Artificial Transmission Line Structures for Tunable Microwave Components and Microwave Sensors*, Shaker, 2011.
- [60] M. Schueler, C. Mandel, M. Puentes, and R. Jakoby, “Metamaterial inspired microwave sensors,” *IEEE Microw. Mag.*, vol. 13, no. 2, pp. 57–68, Mar. 2012.
- [61] J. G. Webster, *The Measurement Instrumentation and Sensors Handbook*. Boca Raton, FL, USA: CRC, 1999.
- [62] J. Fraden, *Handbook of Modern Sensors: Physics, Design, and Applications*, 3rd ed. New York, NY, USA, Springer, 2004.
- [63] J. Naqui, M. Durán-Sindreu, and F. Martín, “Novel Sensors Based on the Symmetry Properties of Split Ring Resonators (SRRs)”, *Sensors*, vol 11, pp. 7545–7553, 2011.
- [64] J. Naqui, M. Durán-Sindreu, and F. Martín, “Alignment and position sensors based on split ring resonators,” *Sensors*, vol. 12, no. 9, pp. 11790–11797, Aug. 2012.
- [65] J. Naqui, M. Durán-Sindreu, and F. Martín, “Transmission lines loaded with bisymmetric resonators and applications,” *IEEE MTT-S Int. Microw. Symp.*, Seattle, WA, USA, Jun. 2013.
- [66] J. Naqui and F. Martín, “Mechanically reconfigurable microstrip lines loaded with stepped impedance resonators and potential applications,” *Int. J. Antennas Propag.*, vol. 2014, ID 346838, 8 pages, Feb. 2014.
- [67] A. Karami-Horestani, C. Fumeaux, S.F. Al-Sarawi, and D. Abbott, “Displacement sensor based on diamond-shaped tapered split ring resonator,” *IEEE Sensors J.*, vol. 13, no. 4, pp. 1153–1160, Apr. 2013.
- [68] A. Horestani, D. Abbott, and C. Fumeaux, “Rotation sensor based on horn-shaped split ring resonator,” *IEEE Sens. J.*, vol. 13, no. 8, pp. 3014–3015, May 2013.
- [69] A. K. Horestani, J. Naqui, D. Abbott, C. Fumeaux, and F. Martín, “Two-dimensional displacement and alignment sensor based on reflection coefficients of open microstrip lines loaded with split ring resonators,” *IET Electron Lett.*, vol. 50, no. 8, pp. 620–622, Apr. 2014.
- [70] J. Naqui and F. Martín, “Transmission lines loaded with bisymmetric resonators and their application to angular displacement and velocity sensors,” *IEEE Trans. Microw. Theory Techn.*, vol. 61, no. 12, pp. 4700–4713, Dec. 2013.
- [71] J. Naqui and F. Martín, “Angular displacement and velocity sensors based on electric-LC (ELC) loaded microstrip lines,” *IEEE Sensors J.*, vol. 14, no. 4, pp. 939–940, Apr. 2014.
- [72] J. Naqui, J. Coromina, A. Karami-Horestani, C. Fumeaux, and F. Martín, “Angular displacement and velocity sensors based on coplanar waveguides (CPWs) loaded with S-shaped split ring resonator (S-SRR)”, *Sensors*, vol. 15, pp. 9628–9650, 2015.
- [73] A. K. Horestani, J. Naqui, Z. Shaterian, D. Abbott, C. Fumeaux, and F. Martín, “Two-dimensional alignment and displacement sensor based on movable broadside-coupled split ring resonators”, *Sensors and Actuators A*, vol. 210, pp. 18–24, Apr. 2014.
- [74] J. Naqui, *et al.*, “Transmission lines loaded with pairs of stepped impedance resonators: modeling and application to differential permittivity measurements”, *IEEE Trans. Microw. Theory Techn.*, vol. 64, no. 11, pp. 3864–3877, Nov. 2016.
- [75] L. Su, J. Mata-Contreras, J. Naqui, and F. Martín, “Splitter/combiner microstrip sections loaded with pairs of complementary split ring resonators (CSRrs): modeling and optimization for differential sensing applications”, *IEEE Trans. Microw. Theory Techn.*, vol. 64(12), pp. 4362–4370, Dec. 2016.
- [76] L. Su, J. Mata-Contreras, P. Vélez, and F. Martín, “Configurations of Splitter/Combiner Microstrip Sections Loaded with Stepped Impedance Resonators (SIRs) for Sensing Applications”, *Sensors*, vol. 16, no. 12, Dec. 2016.
- [77] P. Vélez, L. Su, K. Grenier, J. Mata-Contreras, D. Dubuc, and F. Martín, “Microwave Microfluidic Sensor Based on a Microstrip Splitter/Combiner Configuration and Split Ring Resonators (SRRs) for Dielectric Characterization of Liquids”, *IEEE Sensors J.*, vol. 17, no. 20, pp. 6589–6598, Oct. 2017.
- [78] P. Vélez, J. Mata-Contreras, L. Su, D. Dubuc, K. Grenier, and F. Martín, “Modeling and Analysis of Pairs of Open Complementary Split Ring Resonators (OCSRrs) for Differential Permittivity Sensing”, *2017 IEEE MTT-S International Microwave Workshop Series on Advanced Materials and Processes (IMWS-AMP 2017)*, Pavia, Italy, 20–22 September 2017.
- [79] P. Vélez, K. Grenier, J. Mata-Contreras, D. Dubuc, and F. Martín, “Highly-Sensitive Microwave Sensors Based on Open Complementary Split Ring Resonators (OCSRrs) for Dielectric Characterization and Solute Concentration Measurement in Liquids”, *IEEE Access*, vol. 6, pp. 48324–48338, Aug. 2018.
- [80] P. Vélez, J. Muñoz-Enano, K. Grenier, J. Mata-Contreras, D. Dubuc, and F. Martín, “Split ring resonator (SRR) based microwave fluidic sensor for electrolyte concentration measurements”, *IEEE Sensors J.*, vol. 19, no. 7, pp. 2562–2569, Apr. 2019.
- [81] A. Babajanyan, J. Kim, S. Kim, K. Lee, and B. Friedman, “Sodium chloride sensing by using a near-field microwave microprobe,” *Appl. Phys. Lett.*, vol. 89, no. 18, p. 183504, 2006.
- [82] A. Babajanyan, H. Melikyan, S. Kim, J. Kim, K. Lee, and B. Friedman, “Real-time noninvasive measurement of glucose concentration using a microwave biosensor,” *J. Sensors*, vol. 2010, 2010.
- [83] S. Kim, *et al.*, “Noninvasive in vitro measurement of pig-blood D-glucose by using a microwave cavity sensor,” *Diabetes Res. Clin. Pract.*, vol. 96, no. 3, pp. 379–384, 2012.
- [84] N. Sharafadinzadeh, M. Abdolrazzagh1, and M. Daneshmand, “Highly sensitive microwave split ring resonator sensor using gap extension for glucose sensing”, *2017 IEEE MTT-S International Microwave Workshop Series on Advanced Materials and Processes (IMWS-AMP 2017)*, Pavia, Italy, 20–22 Sep. 2017.
- [85] J. Kim, A. Babajanyan, A. Hovsepian, K. Lee, and B. Friedman, “Microwave dielectric resonator biosensor for aqueous glucose solution”, *Rev. Sci. Instrum.*, vol. 79, paper 086107, 2008.
- [86] D.E. Bockelman and W. R. Eisenstadt, “Combined differential and common-mode scattering parameters: theory and simulation”, *IEEE Trans. Microw. Theory, Techn.*, vol. 43, pp. 1530–1539, Jul. 1995.
- [87] A. Ferrero and M. Pirola, “Generalized mixed-mode S parameters”, *IEEE Trans. Microw. Theory. Techn.*, vol. 54, pp. 458–463, Jan. 2006.
- [88] D.M. Pozar, *Microwave Engineering*, 4th Ed., John Wiley, Hoboken, NJ, 2011.
- [89] J. Muñoz-Enano, P. Vélez, and F. Martín, “Signal balancing in unbalanced transmission lines”, *IEEE Trans. Microw. Theory Techn.*, vol. 67, pp. 3339 – 3349, Aug. 2019.

- [90] M. S. Boybay and O. M. Ramahi, "Material characterization using complementary split-ring resonators," *IEEE Trans. Instrum. Meas.*, vol. 61, no. 11, pp. 3039–3046, Nov. 2012.
- [91] C.-S. Lee and C.-L. Yang, "Complementary split-ring resonators for measuring dielectric constants and loss tangents," *IEEE Microw. Wireless Compon. Lett.*, vol. 24, no. 8, pp. 563–565, Aug. 2014.
- [92] C.-L. Yang, C.-S. Lee, K.-W. Chen, and K.-Z. Chen, "Noncontact measurement of complex permittivity and thickness by using planar resonators," *IEEE Trans. Microw. Theory Techn.*, vol. 64, no. 1, pp. 247–257, Jan. 2016.
- [93] L. Su, J. Mata-Contreras, P. Vélez, and F. Martín, "Estimation of the complex permittivity of liquids by means of complementary split ring resonator (CSRR) loaded transmission lines", *2017 IEEE MTT-S International Microwave Workshop Series on Advanced Materials and Processes (IMWS-AMP 2017)*, Pavia, Italy, 20-22 Sep. 2017.
- [94] L. Su, J. Mata-Contreras, P. Vélez, A. Fernández-Prieto, and F. Martín, "Analytical method to estimate the complex permittivity of oil Samples", *Sensors*, 18(4), paper 984, 2018.
- [95] T. Chretiennot, D. Dubuc, and K. Grenier, "A Microwave and Microfluidic Planar Resonator for Efficient and Accurate Complex Permittivity Characterization of Aqueous Solutions," *IEEE Trans. Microw. Theory Techn.*, vol. 61, no. 2, pp. 972-978, Feb. 2013.
- [96] A. Ebrahimi, W. Withayachumnankul, S. Al-Sarawi, and D. Abbott, "High-Sensitivity Metamaterial-Inspired Sensor for Microfluidic Dielectric Characterization," *IEEE Sensors J.*, vol. 14, no. 5, pp. 1345-1351, May 2014.
- [97] W. Withayachumnankul, K. Jaruwongrunsee, A. Tuantranont, C. Fumeaux, and D. Abbott, "Metamaterial-based microfluidic sensor for dielectric characterization", *Sensors and Actuators A, Physical*, vol. 189, pp. 233-237, 2013.
- [98] A. Salim and S. Lim, "Complementary split-ring resonator-loaded microfluidic ethanol chemical sensor", *Sensors*, vol. 16, Oct. 2016.
- [99] M. Abdolrazzagli, M. Daneshmand, and A. K. Iyer, "Strongly Enhanced Sensitivity in Planar Microwave Sensors Based on Metamaterial Coupling," *IEEE Trans. Microw. Theory Techn.*, vol. 66, no. 4, pp. 1843-1855, Apr. 2018.
- [100] B. D. Wiltshire and M. H. Zarifi, "3-D Printing Microfluidic Channels With Embedded Planar Microwave Resonators for RFID and Liquid Detection," *IEEE Microw. Wireless Compon. Lett.*, vol. 29, no. 1, pp. 65-67, Jan. 2019.
- [101] X. Zhang, C. Ruan, T. ul Haq, and K. Chen, "High-Sensitivity Microwave Sensor for Liquid Characterization Using a Complementary Circular Spiral Resonator", *Sensors*, vol. 19, Feb. 2019.
- [102] J. Kilpijärvi, N. Halonen, J. A. Juuti, and J. Hannu, "Microfluidic Microwave Sensor for Detecting Saline in Biological Range", *Sensors*, vol. 19, Feb. 2019.
- [103] P. Vélez, J. Muñoz-Enano, M. Gil, J. Mata-Contreras, and F. Martín, "Differential Microfluidic Sensors Based on Dumbbell-Shaped Defect Ground Structures in Microstrip Technology: Analysis, Optimization, and Applications", *Sensors*, vol. 19, no. 14, pp. 3189, Jul. 2019.
- [104] A. Ebrahimi, J. Scott, and K. Ghorbani, "Transmission Lines Terminated With LC Resonators for Differential Permittivity Sensing," *IEEE Microw. Wireless Compon. Lett.*, vol. 28, no. 12, pp. 1149-1151, Dec. 2018.
- [105] A. Ebrahimi, J. Scott, and K. Ghorbani, "Differential Sensors Using Microstrip Lines Loaded With Two Split-Ring Resonators," *IEEE Sensors J.*, vol. 18, no. 14, pp. 5786-5793, 15 Jul. 2018.
- [106] J. Selga, J. Coromina, P. Vélez, A. Fernández-Prieto, J. Bonache, and F. Martín, "Miniaturised and harmonic-suppressed rat-race couplers based on slow-wave transmission lines", *IET Microw. Ant. Propag.*, vol. 13, no. 9, pp. 1293-1299, Jul. 2019.



Jonathan Muñoz-Enano was born in Mollet del Vallès (Barcelona), Spain, in 1994. He received the Bachelor's Degree in Electronic Telecommunications Engineering in 2016 and the Master's Degree in Telecommunications Engineering in 2018, both at the Autonomous University of Barcelona (UAB). Actually, he is working in the same university in the elaboration of his PhD, which is focused on the development of microwave sensors based on metamaterials concepts for the dielectric characterization of materials and biosensors.



Paris Vélez (S'10–M'14) was born in Barcelona, Spain, in 1982. He received the degree in Telecommunications Engineering, specializing in electronics, the Electronics Engineering degree, and the Ph.D. degree in Electrical Engineering from the Universitat Autònoma de Barcelona, Barcelona, in 2008, 2010, and 2014, respectively. His Ph.D. thesis concerned common mode suppression differential microwave circuits based on metamaterial concepts and semi-lumped resonators. During the Ph.D., he was awarded with a pre-doctoral teaching and research fellowship by the Spanish Government from 2011 to 2014. From 2015-2017, he was involved in the subjects related to metamaterials sensors for fluidics detection and characterization at LAAS-CNRS through a TECNIOSpring fellowship cofounded by the Marie Curie program. His current research interests include the miniaturization of passive circuits RF/microwave and sensors-based metamaterials through Juan de la Cierva fellowship. Dr. Vélez is a Reviewer for the IEEE Transactions on Microwave Theory and Techniques and for other journals.



Marta Gil Barba (S'05–M'09) was born in Valdepeñas, Ciudad Real, Spain, in 1981. She received the Physics degree from Universidad de Granada, Spain, in 2005, and the Ph.D. degree in electronic engineering from the Universitat Autònoma de Barcelona, Barcelona, Spain, in 2009. She studied one year with the Friedrich Schiller Universität Jena, Jena, Germany. During her PhD Thesis she was holder of a METAMORPHOSE NoE grant and National Research Fellowship from the FPU Program of the Education and Science Spanish Ministry. As a postdoctoral researcher, she was awarded with a Juan de la Cierva fellowship working in the Universidad de Castilla-La Mancha. She was postdoctoral researcher in the Institut für Mikrowellentechnik und Photonik in Technische Universität Darmstadt and in the Carlos III University of Madrid. She is currently assistant professor in the Universidad Politécnica de Madrid. She has worked in metamaterials, piezoelectric MEMS and microwave passive devices. Her current interests include metamaterials sensors for fluidic detection.



Javier Mata-Contreras was born in 1976 in Málaga (Spain). He received the Ingeniería de Telecomunicación Degree from the Universidad de Málaga (UMA) in 2000 and the PhD degree from the same university in 2010, with the Thesis "Distributed Amplifiers and Mixers with Transmission Lines based on Metamaterials". In 2000, he joined the UMA Department of Ingeniería de Comunicaciones UMA as Assistant Professor. He is currently working at CIMITEC and the Universitat Autònoma de Barcelona as Visitant Professor. His research interests include active and passive microwave devices and active distributed circuits based on metamaterials, among others.



Ferran Martín (M'04–SM'08–F'12) was born in Barakaldo (Vizcaya), Spain in 1965. He received the B.S. Degree in Physics from the Universitat Autònoma de Barcelona (UAB) in 1988 and the PhD degree in 1992. From 1994 up to 2006 he was Associate Professor in Electronics at the Departament d'Enginyeria Electrònica (Universitat Autònoma de Barcelona), and since 2007 he is Full Professor of Electronics. In recent years, he has been involved in different research activities including modelling and simulation of electron devices for high frequency applications, millimeter wave and THz generation systems, and the application of electromagnetic bandgaps to microwave and millimeter wave circuits. He is now very active in the field of metamaterials and their application to the miniaturization and optimization of microwave circuits and antennas. Other topics of interest include microwave sensors and RFID systems, with special emphasis on the development of high data capacity chipless-RFID tags. He is the head of the Microwave Engineering, Metamaterials and Antennas Group (GEMMA Group) at UAB, and director of CIMITEC, a research Center on Metamaterials supported by TECNIO (Generalitat de Catalunya). He has organized several international events related to metamaterials and related topics, including Workshops at the IEEE International Microwave Symposium (years 2005 and 2007) and European Microwave Conference (2009, 2015 and 2017), and the Fifth International Congress on Advanced Electromagnetic Materials in Microwaves and Optics (Metamaterials 2011), where he has

acted as chair of the Local Organizing Committee. He has acted as Guest Editor for five Special Issues on Metamaterials and Sensors in five International Journals. He has authored and co-authored over 550 technical conference, letter, journal papers and book chapters, he is co-author of the book on Metamaterials entitled *Metamaterials with Negative Parameters: Theory, Design and Microwave Applications* (John Wiley & Sons Inc.), author of the book *Artificial Transmission Lines for RF and Microwave Applications* (John Wiley & Sons Inc.), and co-editor of the book *Balanced Microwave Filters* (John Wiley & Sons Inc.). Ferran Martín has generated 19 PhDs, has filed several patents on metamaterials and has headed several Development Contracts.

Prof. Martín is a member of the IEEE Microwave Theory and Techniques Society (IEEE MTT-S). He is reviewer of the IEEE Transactions on Microwave Theory and Techniques and IEEE Microwave and Wireless Components Letters, among many other journals, and he serves as member of the Editorial Board of IET Microwaves, Antennas and Propagation, International Journal of RF and Microwave Computer-Aided Engineering, and Sensors. He is also a member of the Technical Committees of the European Microwave Conference (EuMC) and International Congress on Advanced Electromagnetic Materials in Microwaves and Optics (Metamaterials). Among his distinctions, Ferran Martín has received the 2006 Duran Farell Prize for Technological Research, he holds the *Parc de Recerca UAB – Santander* Technology Transfer Chair, and he has been the recipient of three ICREA ACADEMIA Awards (calls 2008, 2013 and 2018). He is Fellow of the IEEE and IET.